IOP Publishing Superconductor Science and Technology
Supercond. Sci. Technol. 31 (2018) 105002 (6pp) https://doi.org/10.1088/1361-6668/aad790

Crystal structure determination under high pressure in the iron-based ladder superconductor $BaFe_2S_3$

Kensuke Kobayashi[1], Sachiko Maki[2], Youichi Murakami[1,3], Yasuyuki Hirata[4], Kenya Ohgushi[5] and Jun-ichi Yamaura[2]

[1] Condensed Matter Research Center, Institute of Materials Structure Science, High Energy Accelerator Research Organization (KEK), Tsukuba, Ibaraki 305-0801, Japan
[2] Materials Research Center for Element Strategy, Tokyo Institute of Technology, Yokohama, Kanagawa 226-8503, Japan
[3] Department of Materials Structure Science, The Graduate University for Advanced Studies, Tsukuba, Ibaraki 305-0801, Japan
[4] Institute for Solid State Physics, The University of Tokyo, Kashiwa, Chiba 277-8581, Japan
[5] Department of Physics, Tohoku University, Sendai, Miyagi 980-8578, Japan

E-mail: jyamaura@mces.titech.ac.jp

Received 1 May 2018, revised 24 July 2018
Accepted for publication 2 August 2018
Published 28 August 2018

Abstract

The crystal structure of $BaFe_2S_3$ is determined up to ~12 GPa by means of x-ray powder diffraction experiments using synchrotron radiation at room temperature. $BaFe_2S_3$ is the first superconductor in iron-based ladder compounds, showing the critical temperature at $T_c = 24$ K under 11.6 GPa. The superconductivity emerges on the application of pressure after suppressing an antiferromagnetic Mott insulating state. The atomic positions in the superconducting state remain hitherto unknown experimentally. We found significant changes of structural parameters: shrinkage of the Fe-ladder unit and decreasing height of the S atom position from the Fe plane. Moreover, a reduction of the S–S distance between the ladders was observed under pressure. The pressure dependence of the structural parameters is strikingly different from the prediction of the band calculation.

Keywords: iron-based ladder, superconductor, structure determination, high pressure

(Some figures may appear in colour only in the online journal)

1. Introduction

A family of iron-based superconductors with high critical temperature T_c has been vigorously studied since its discovery in 2008 [1–4]. All materials in this family comprise a 2D conduction layer made of $FePn_4$ (Pn = pnictogen) tetrahedral units. They exhibit superconductivity upon carrier doping and/or application of pressure in place of an antiferromagnetic ordered state [2, 3]. The origin of the superconductivity has been primarily interpreted as having been derived from spin- and orbital-fluctuations enhanced by a Fermi surface nesting. Namely, an itinerant picture is regarded as a starting point [5–7].

The AFe_2X_3 (A = K, Rb, Cs and Ba; X = S, Se and Te) series has a $CsCu_2Cl_3$-type structure with two-leg Fe ladders consisting of edge-shared FeX_4 tetrahedral units, as shown in figure 1 [8–11]. Hence, ladder-type iron-based materials are viewed as a cousin of the 2D iron-based superconductor (2dFeSC). Iron-based ladder compounds are Mott insulators that exhibit stripe- or block-type antiferromagnetic ordered states [12–20]. Stripe types of Fe-spin arrangements are widely observed among the parent compounds of 2dFeSCs [21–24]. Iron-based ladders exhibit antiferromagnetic transitions at T_N = 110–255 K with magnetic moments of m_{Fe} = 1.2–2.8 μ_B [12–18]. The relatively large moments suggest that electrons have more

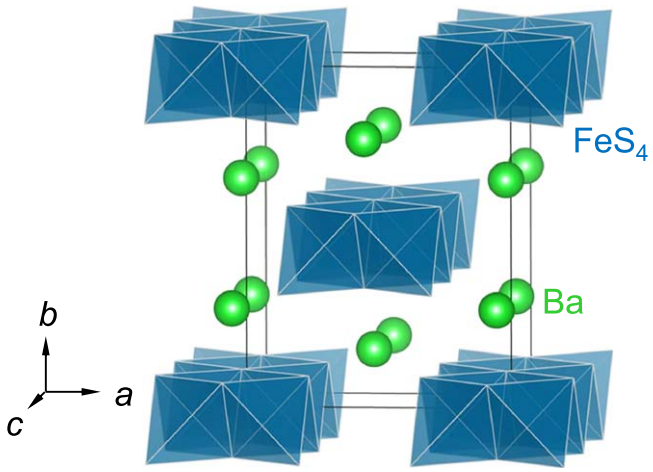

Figure 1. Crystal structure of $BaFe_2S_3$. A ladder made of edge-shared FeS_4 tetrahedra runs along the *c*-axis. The green balls represent Ba atoms. The structure is drawn using VESTA software [11].

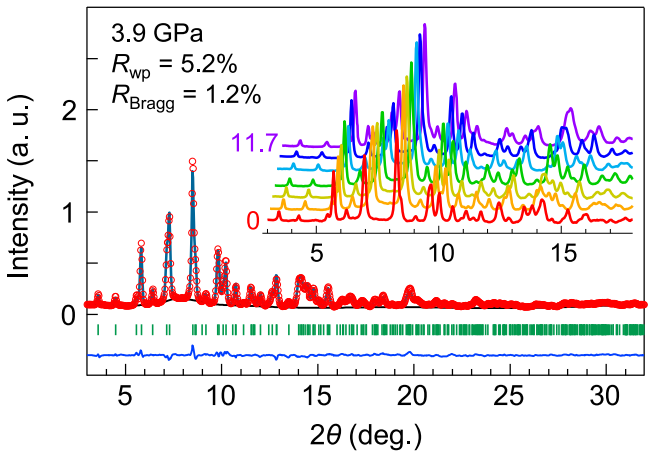

Figure 2. X-ray powder diffraction pattern of $BaFe_2S_3$ under 3.9 GPa at 300 K. Observed (red circle), calculated (blue green line), difference profiles (blue line) and positions of the Bragg peaks (green ticks) are plotted. Inset shows the diffraction patterns under 0, 2.8, 3.9, 5.5, 8.1, 9.3 and 11.7 GPa with the 2θ offset of 0, +0.1, +0.2, +0.3, +0.4, +0.5 and +0.6, respectively.

localized character in the ladder systems than in the 2dFeSCs.

Recently, Takahashi *et al* have demonstrated a pressure-induced superconductivity in $BaFe_2S_3$, and Yamauchi *et al* have further investigated the details of this superconductivity [16, 25]. $BaFe_2S_3$ behaves as an insulator throughout the entire temperature range at ambient pressure. This shows possible orbital ordering transition at $T_s = 200$ K [25, 26] and undergoes a stripe-type antiferromagnetic ordering at $T_N = 110$ K [16]. The application of pressure suppresses these ordered states and the superconductivity emerges immediately after T_N vanishes at 9 GPa. Eventually, T_c reaches 24 K at 11.6 GPa [25]. The possible origins of superconductivity have been discussed in the light of spin fluctuations enhanced by the Fermi surface nesting, a charge transfer from S to Fe atoms and a strong electron correlation

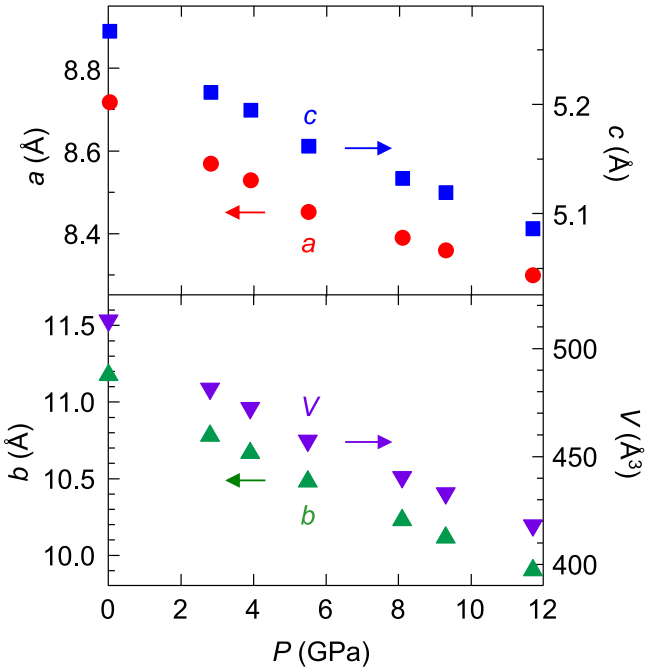

Figure 3. Lattice constants *a*, *b* and *c* and unit cell volume *V* as a function of pressure for $BaFe_2S_3$.

in the vicinity of the Mott transition. However, its origin remains a controversial subject [16, 25, 27–32].

The crystal structures of $BaFe_2S_3$ under pressure have been investigated experimentally concerning the lattice constants up to ~17 GPa and the atomic positions up to 1.3 GPa [16, 18]. Moreover, the atomic positions up to 12 GPa were calculated theoretically [29]. However, the atomic positions within the superconducting phase remain undetermined experimentally. In this study, we determined the details of the crystal structure in $BaFe_2S_3$ up to ~12 GPa. We found a substantial shrinkage of the Fe-ladder unit, significant lowering in the S atom height from the Fe plane and an unexpected large reduction in the S–S distance between the ladder units under high pressure. These may involve the significant reduction of the localized character of the electrons in the present compound and thereby entail superconductivity.

2. Experiments

$BaFe_2S_3$ samples were prepared by a solid-state reaction, as reported in the literature [33]. Synchrotron x-ray powder diffraction measurement was performed at 300 K at NE1A of PF-AR at the High Energy Accelerator Research Organization (KEK). Pressure up to ~12 GPa was applied using a diamond anvil cell with 600 μm culet anvils and a SUS301T gasket with a 300 μm hole. The anvils are supported by the 45° tapered window without a backing plate, which realizes the reduction of background scatter and simplifies the absorption correction of the diamond, as employed in previous work [34].

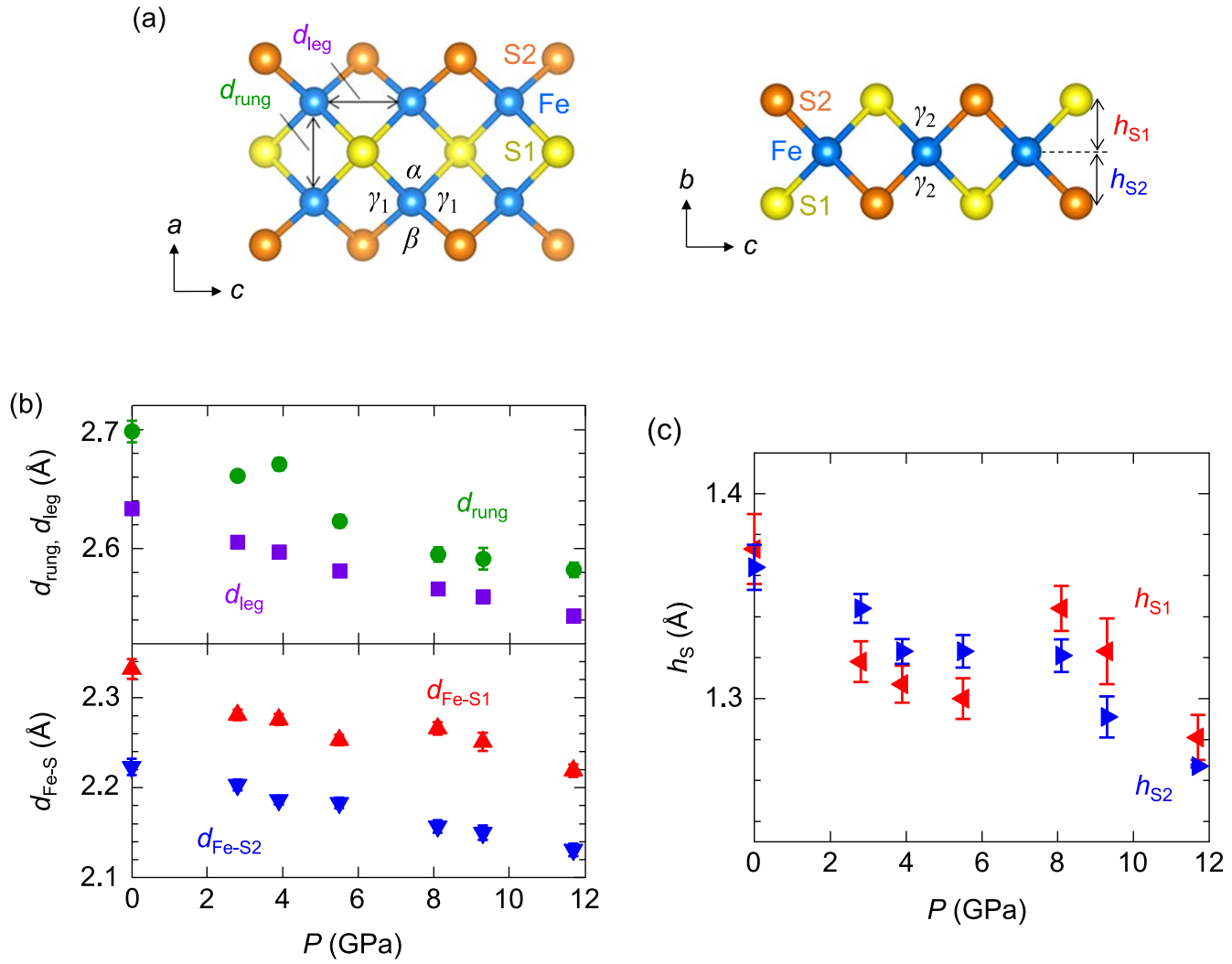

Figure 4. (a) $BaFe_2S_3$ ladder units of the upper (left) and side views (right). (b) Pressure dependence of Fe–Fe distances d_{rung} and d_{leg} and Fe–S bond distance $d_{Fe–S}$. (c) Pressure dependence of S atom height h_S from the Fe plane. Superconductivity emerges above 9 GPa after the suppression of the magnetically ordered state.

The 2D images were collected using a diffractometer (Rigaku R-Axis) with a curved imaging plate at the wavelength of $\lambda = 0.420\,103$ Å. The images were integrated to yield 2θ-intensity data on Rigaku Display software. A methanol-ethanol mixture with a ratio of 4:1 was used as a pressure transmitting medium, and the pressure was determined by ruby fluorescence measurement [35].

The crystal structures were determined using the Rietveld method on RIETAN-FP software [36] according to the structure at ambient pressure indexed to the space group of *Cmcm*, as described in the literature [8]. The reliability factor in the refinements converged at $R_{wp} = 6.9$, 4.9, 5.2, 6.9, 6.4, 6.7 and 7.2% and $R_{Bragg} = 1.9$, 2.8, 1.2, 2.5, 3.1, 2.5. and 4.7% for the data under 0, 2.8, 3.9, 5.5, 8.1, 9.3 and 11.7 GPa, respectively [36]. Figure 2 represents the x-ray pattern with the refinement at 3.9 GPa, and all x-ray patterns taken in this work are indicated in the inset. Although we observed a little broadening above the glass transition of the ethanol–methanol mixture at 10.5 GPa [37], the structural analysis converged sufficiently under 11.7 GPa.

3. Results and discussion

Figure 3 shows the lattice constants of $BaFe_2S_3$ as a function of pressure at 300 K. The two-leg ladder of Fe atoms runs along the *c*-axis, and Ba atoms are allocated in between the ladders (figure 1). All the lattice constants decrease monotonically. The values of linear compressibility at low-pressure range are estimated to be $k_a = 5.52 \times 10^{-3}\,GPa^{-1}$ (rung direction), $k_b = 11.3 \times 10^{-3}\,GPa^{-1}$ (interlayer direction) and $k_c = 3.62 \times 10^{-3}\,GPa^{-1}$ (leg direction). This indicates that the crystal is squeezed anisotropically by pressure. These values are in good agreement with the previous literature [16, 18]. The values of compressibility for another pressure-induced ladder-superconductor $Sr_{0.4}Ca_{13.6}Cu_{24}O_{41+\delta}$ (T_c = 13 K, 3 GPa) were previously obtained to be $k_a = 0.8 \times 10^{-3}\,GPa^{-1}$ (rung direction), $k_b = 7.3 \times 10^{-3}\,GPa^{-1}$ (interlayer direction) and $k_c = 2.2 \times 10^{-3}\,GPa^{-1}$ (leg direction) [38–40]. In $BaFe_2S_3$, the values of compressibility are relatively larger than those of $Sr_{0.4}Ca_{13.6}Cu_{24}O_{41+\delta}$. In $BaFe_2S_3$, the lattice constant *b*, which is the stacking direction

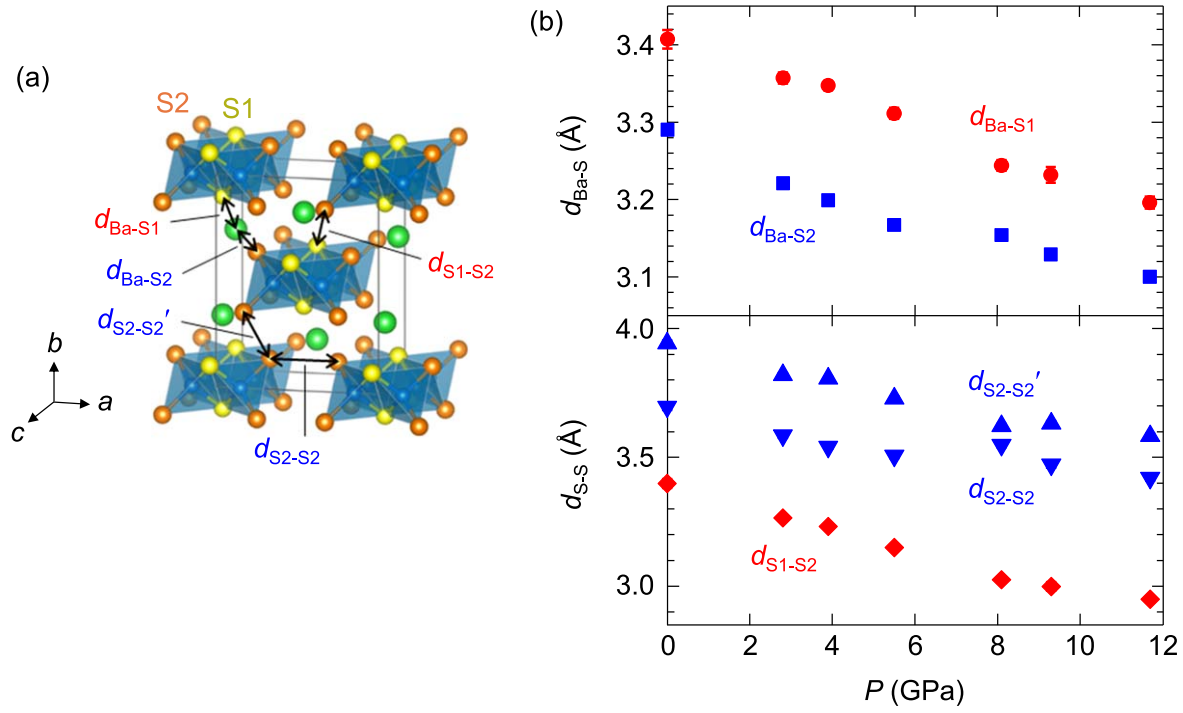

Figure 5. (a) Crystal structure and the definition of the inter-ladder distances. (b) Pressure dependence of Ba–S distances $d_{Ba–S1}$ and $d_{Ba–S2}$, and the S–S distance between neighboring ladder units $d_{S1–S2}$, $d_{S2–S2}$ and $d_{S2–S2}'$.

of the ladder, indicates a considerable decrease as large as 11.4% from 0 to 11.7 GPa. The bulk modulus (B_0) is estimated to be 46 GPa using the empirical Murnaghan equation of state: $V/V_0 = (1 + p(B'_0/B_0))^{-1/B'0}$, where V_0 is the volume at ambient pressure and B'_0 is fixed at 4.2 [34, 41].

Figure 4(a) illustrates the $BaFe_2S_3$ ladder units. The ladder is symmetric along the rung and leg directions because the mirror planes perpendicular to the Fe plane are located on the S1 atoms. Here, we demonstrate the crystal parameters based on the structural refinement under pressure. The Fe–Fe distances d_{rung} and d_{leg} and the Fe–S bond distance $d_{Fe–S}$ are plotted in figure 4(b). At ambient pressure, the d_{rung} and d_{leg} are 2.698(9) and 2.6333(4) Å, respectively. Their average value is approximately 7% shorter than that in LaFeAsO of 2dFeSC [34]. Although $BaFe_2S_3$ has a shorter Fe–Fe length than that in LaFeAsO, the correlation effect is considered stronger, which presumably stems from the stronger quasi-one-dimensionality in $BaFe_2S_3$. The d_{rung} and d_{leg} diminish monotonically on the application of pressure, and the variations against pressure are -0.014 Å GPa^{-1} for d_{rung} and -0.010 Å GPa^{-1} for d_{leg} at low-pressure range. The ratio of leg-to-rung distances d_{leg}/d_{rung} changes slightly from 0.976 at 0 GPa to 0.985 at 11.7 GPa. The outlier value of d_{rung} at 3.9 GPa on the monotonic pressure dependence is thought to be non-intrinsic.

The $d_{Fe–S2}$ decreases monotonically on the application of pressure, while the $d_{Fe–S1}$ involves non-monotonic behavior. The variations against pressure up to 5.5 GPa are estimated to be -0.014 Å GPa^{-1} for $d_{Fe–S1}$ and -0.007 Å GPa^{-1} for $d_{Fe–S2}$. The variation in $d_{Fe–S1}$ is quite large compared with -0.007 Å GPa^{-1} for $d_{Fe–As}$ in LaFeAsO [34]. The bond angles of FeS_4 are $\alpha = 109.3(3)°$, $\beta = 117.0(4)°$, $\gamma_1 = 109.20(8)°$ and $\gamma_2 = 105.98(8)°$ at 0 GPa, and $\alpha = 108.8(2)°$, $\beta = 114.8(3)°$, $\gamma_1 = 108.35(8)°$ and $\gamma_2 = 108.19(8)°$ at 11.7 GPa, where α, β and γ are the angles for S1–Fe–S1, S2–Fe–S2 and S1–Fe–S2, respectively (see figure 4(a)). The bond angle variance σ^2, which indicates a deviation from the regular tetrahedron of FeS_4, changes from $\sigma^2 = 16.4(27)$ degrees^2 at 0 GPa to $\sigma^2 = 6.9(14)$ degrees^2 at 11.7 GPa [42]. Hence, the FeS_4 tetrahedron varies towards the regular one on the application of pressure.

Figure 4(c) displays the S atom height h_S from the iron plane. The h_{S2} indicates the monotonic decreasing on the application of pressure, while the h_{S1} involves non-monotonic behavior similar to the pressure dependence of the $d_{Fe–S1}$. The variations against pressure up to 5.5 GPa are estimated to be -0.013 Å GPa^{-1} for h_{S1} and -0.007 Å GPa^{-1} for h_{S2}. The variations in h_{S1} and h_{S2} are quite large compared with -0.004 Å GPa^{-1} for h_{As} in LaFeAsO [34]. Eventually, the h_{S1} and h_{S2} exhibit large decreases of 7% from 0 to 11.7 GPa. The resistivity changes from insulating to semi-metallic behavior at around 7 GPa near room temperature. Moreover, the superconductivity appears above 9 GPa [25]. Thus, the non-monotonic behavior in h_{S1} may be related to a certain change in the electronic state. We note the crucial difference between the measured and calculated values in h_{S1} [29]. Moreover, the calculation could not detect the non-monotonic behavior of h_{S1}, as mentioned above. Since the values of h_S are strongly associated with the electronic states through the Fe-3*d* and S-3*p* hybridization [5, 6, 27], further theoretical studies will be required in future.

We next focus on the inter-ladder coupling of $BaFe_2S_3$. Figure 5(a) represents the crystal structure of $BaFe_2S_3$ with the definition of inter-ladder distances. The Ba–S distances $d_{Ba–S1}$ and $d_{Ba–S2}$, and the S–S distances $d_{S1–S2}$, $d_{S2–S2}$, and

the $d_{S2-S2}{}'$ are plotted in figure 5(b). Using the ionic radii of $r_{Ba} = 1.42$ Å for Ba and $r_S = 1.84$ Å for S [43], the sums of their values are $r_{Ba} + r_S = 3.26$ Å and $r_S + r_S = 3.68$ Å. At ambient pressure, the inter-ladder distances are tailored to the hard sphere model based on the ionic radii. On the application of pressure, all the inter-ladder parameters show considerable decreases. Eventually, the inter-ladder S–S distance indicates $d_{S1-S2} = 2.95(1)$ Å at 11.7 GPa. Thus, the distance surpasses the normal limits of the sphere packing. Therefore, we suggest that the strong inter-ladder contraction under high pressure introduces the one-dimensionality weakened in $BaFe_2S_3$.

Finally, let us consider the interplay between the structure and the electronic state under pressure. The ground state of this compound at ambient pressure is interpreted as the orbital selective Mott insulator with strong electron correlation [31, 32]. We identified the substantial response to pressure: the shrinkage of the Fe-ladder unit and the reduction of h_S on the application of pressure. It is thus plausible that these factors enhance the mixing of the Fe and S atom orbitals, which may induce the enlarged Fe-3*d* bandwidth. Moreover, the possible increase of dimensionality under pressure also works to reduce the localized character, which is presumably related to the triggering of the superconductivity under pressure.

4. Summary

We investigated the crystal structure of the iron-based ladder superconductor $BaFe_2S_3$. The superconductivity emerged above 9 GPa; T_c reached its maximum at the value of 24 K at 11.6 GPa. We found notable pressure effects: the large shrinkage of the Fe-ladder unit, the considerable decrease in the S atom height and significant enhancement of the S–S contact between the ladders. These findings suggest that the Fe-3*d* and S-3*p* hybridization and the one-dimensionality weakened, inducing a significant change of the band structure under high pressure, which triggers the emergence of superconductivity. Since there are crucial differences for the atomic positions as well as their pressure dependence between the experimental and calculation results, more detailed discussion awaits the electronic-state calculation and the optical conductivity measurement under pressure.

Acknowledgments

We would like to thank Y Kuramoto, H Takahashi and T Yamauchi for their fruitful discussions. This work was supported by MEXT Element Strategy Initiative to Form Core Research Center and JSPS KAKENHI (Nos. 16K05434, 16H04019, 16H01062, 18H01159, and 18H04302). The XRD study was performed with the approval of the Photon Factory Program Advisory Committee (No. 2016S2-004) and the Large Scale Simulation Program (No. 16/17-18 (FY2017)) at KEK.

ORCID iDs

Jun-ichi Yamaura https://orcid.org/0000-0002-8992-9099

References

[1] Kamihara Y, Watanabe T, Hirano M and Hosono H 2008 *J. Am. Chem. Soc.* **130** 3296
[2] Paglione J and Greene R J 2010 *Nat. Phys.* **6** 645
[3] Stewart G R 2011 *Rev. Mod. Phys.* **83** 1589
[4] Hosono H and Kuroki K 2015 *Physica* C **514** 399
[5] Kuroki K, Usui H, Onari S, Arita R and Aoki H 2009 *Phys. Rev.* B **79** 224511
[6] Usui H and Kuroki K 2011 *Phys. Rev.* B **84** 024505
[7] Kontani H, Saito T and Onari S 2011 *Phys. Rev.* B **84** 024528
[8] Hong H Y and Steinfink H 1972 *J. Solid State Chem.* **5** 93
[9] Klepp K O, Sparlinek W and Boller H 1996 *J. Alloys Compd.* **238** 1
[10] Mitchell R H, Ross K C and Potter E G 2004 *J. Solid State Chem.* **177** 1867
[11] Momma K and Izumi F 2011 *J. Appl. Crystallogr.* **44** 1272
[12] Caron J M, Neilson J R, Miller D C, Llobet A and McQueen T M 2011 *Phys. Rev.* B **84** 180409(R)
[13] Du F, Ohgushi K, Nambu Y, Kawakami T, Avdeev M, Hirata Y, Watanabe Y, Sato T J and Ueda Y 2012 *Phys. Rev.* B **85** 214436
[14] Nambu Y *et al* 2012 *Phys. Rev.* B **85** 064413
[15] Caron J M, Neilson J R, Miller D C, Arpino K, Llobet A and McQueen T M 2012 *Phys. Rev.* B **85** 180405(R)
[16] Takahashi H *et al* 2015 *Nat. Mater.* **14** 1008
[17] Mourigal M, Wu S, Stone M B, Neilson J R, Caron J M, McQueen T M and Broholm C L 2015 *Phys. Rev. Lett.* **115** 047401
[18] Chi S, Uwatoko Y, Cao H, Hirata Y, Hashizume K, Aoyama T and Ohgushi K 2016 *Phys. Rev. Lett.* **117** 047003
[19] Luo Q *et al* 2013 *Phys. Rev.* B **87** 024404
[20] Dong S, Liu J-M and Dagotto E 2014 *Phys. Rev. Lett.* **113** 187204
[21] Lumsden M D and Christianson A D 2010 *J. Phys.: Condens. Matter* **22** 203203
[22] Qureshi N, Drees Y, Werner J, Wurmehl S, Hess C, Klingeler R, Büchner B, Fernández-Díaz M T and Braden M 2010 *Phys. Rev.* B **82** 184521
[23] Hiraishi M *et al* 2014 *Nat. Phys.* **10** 300
[24] Huang Q, Qiu Y, Bao W, Green M A, Lynn J W, Gasparovic Y C, Wu T, Wu G and Chen X H 2008 *Phys. Rev. Lett.* **101** 257003
[25] Yamauchi T, Hirata Y, Ueda Y and Ohgushi K 2015 *Phys. Rev. Lett.* **115** 246402
[26] Takubo K *et al* 2017 *Phys. Rev.* B **96** 115157
[27] Arita R, Ikeda H, Sakai S and Suzuki M 2015 *Phys. Rev.* B **92** 054515
[28] Zhang Y, Lin L, Zhang J-J, Dagotto E and Dong S 2017 *Phys. Rev.* B **95** 115154
[29] Suzuki M-T, Arita R and Ikeda H 2015 *Phys. Rev.* B **92** 085116
[30] Lv W, Moreo A and Dagotto E 2013 *Phys. Rev.* B **88** 094508
[31] Patel N D, Nocera A, Alvarez G, Arita R, Moreo A and Dagotto E 2016 *Phys. Rev.* B **94** 075119
[32] Patel N D, Nocera A, Alvarez G, Moreo A and Dagotto E 2017 *Phys. Rev.* B **96** 024520
[33] Hirata Y, Maki S, Yamaura J, Yamauchi T and Ohgushi K 2015 *Phys. Rev.* B **92** 205109
[34] Kobayashi K, Yamaura J, Iimura S, Maki S, Sagayama H, Kumai R, Murakami Y, Takahashi H, Matsuishi S and Hosono H 2016 *Sci. Rep.* **6** 39646
[35] Ragan D D, Gustavsen R and Schiferl D 1992 *J. Appl. Phys.* **72** 5539

[36] Izumi F and Momma K 2007 *Solid State Phenom.* **130** 15
[37] Klotz S, Chervin J-C, Munsch P and Marchand G L 2009 *J. Phys. D: Appl. Phys.* **42** 075413
[38] Uehara M, Nagata T, Akimitsu J, Takahashi H, Môri M and Kinoshita K 1996 *J. Phys. Soc. Jpn.* **65** 2764
[39] Isobe M, Ohta T, Onoda M, Izumi F, Nakano S, Li J Q, Matsui Y, Takayama-Muromachi E, Matsumoto T and Hayakawa H 1998 *Phys. Rev.* B **57** 613
[40] Pachot S, Bordet P, Cava R J, Chaillout C, Darie C, Hanfland M, Marezio M and Takagi H 1999 *Phys. Rev.* B **59** 12048
[41] Garbarino G, Weht R, Sow A, Sulpice A, Toulemonde P, Álvarez-Murga M, Strobel P, Bouvier P, Mezouar M and Núñez-Regueiro M 2011 *Phys. Rev.* B **84** 024510
[42] Robinson K, Gibbs G V and Ribbe P H 1971 *Science* **172** 567
[43] Shannon R D 1976 *Acta Crystallogr.* A **32** 751